Neural Network Wind Retrieval from ERS-1 Scatterometer Data

P. Richaume[1], F. Badran[2], M. Crepon[1], C. Mejía[1], H. Roquet[3], S. Thiria[1]

[1] Laboratoire d'Océanographie Dynamique et Climatologie, Université Paris VI, Paris, France

[2] Chaire de Recherche Opérationnelle, CNAM, Paris, France

[3] Météo-France SCEM/CMS, Lannion, France

(final version)

Abstract

This paper presents a neural network methodology to retrieve wind vectors from ERS1 scatterometer data. First a neural network (NN-INVERSE) computes the most probable wind vectors. Probabilities for the estimated wind direction are given. At least 75 % of the most probable wind directions are consistent with ECMWF winds (at ± 20°). Then the remaining ambiguities are resolved by an adapted PRESCAT method that uses the probabilities provided by NN-INVERSE. Several statistical tests are presented to evaluate the skill of the method. The good performance is mainly due to the use of a spatial context and to the probabilistic approach adopted to estimate the wind direction. Comparisons with other methods are also presented. The good performance of the neural network method suggests that a self-consistent wind retrieval from ERS1 Scatterometer is possible.

1. Introduction

Most methods which extract wind vectors from scatterometer measurements (sigma-0) are based on a local inversion of a Geophysical Model Function (GMF) modeling the response of the scatterometer, sigma-0, as a function of wind vector and incidence angle. For each measurement cell, wind retrieval algorithms compute the wind vector by minimizing the difference between the observed sigma-0 and the sigma-0 computed by using a GMF with respect to an appropriate cost function (Stoffelen and Anderson, 1997a). For ERS1/2 scatterometers the existing GMFs show that the surface defined by the function giving the wind vector in the $(\sigma_1, \sigma_2, \sigma_3)$ space is a two-sheathed cone-like surface whose intersections correspond to ambiguities in the wind azimuths **(Fig. 1 a** and **b)** (Cavanie and Offiler, 1986, Stoffelen and Anderson 1997a). A coordinate along the generatrix is a function of the wind speed while a section crossing the cone is a Lissajous like curve which is a function of the wind azimuth. At a constant wind speed, the Lissajous like curve implies that two azimuths differing by 180° are possible for some sigma-0 triplets. Noise dramatically increases the ambiguity regions. From a geometrical point of view, the wind retrieval consists in finding the point on the conic surface whose distance to the sigma-0 triplets is a minimum (Stoffelen and Anderson, 1997a). The physical coordinates on the conic surface with respect to the wind vector parameters are the wind speed and the wind direction. Thus, it seems natural to choose these parameters in the wind retrieval procedure as most algorithms do. Those algorithms propose different possible wind azimuths for each wind vector cell of the swath but are unable to choose the actual one without external information. In classical wind retrieval schemes this ambiguity is removed by adjusting the direction of the retrieved wind vectors to those provided by numerical weather prediction models (NWP). A final wind field, which gives the correct direction of the wind vector, is then obtained.

In the following we present an alternative method using neural networks (NN) which provides wind fields from ERS-1 measurements. This methodology is based on the feasibility study of Thiria *et al* (1993) performed on simulated data before the launch of ERS-1. It consists of two separate phases: the first one inverts the ERS-1 measurements and provides ambiguous wind vectors (NN-INVERSE), and the second one removes the wind direction ambiguities. The major difference with the existing methods is that NN-INVERSE is a transfer function mapping the sigma-0 directly to the wind vectors. The NN-INVERSE is an explicit model represented by an algebraic function that does not require a minimization of a GMF functional for each wind vector cell as in most of the existing methods. The two major advantages are:

- the obtained function is directly differentiable and gives access to sensitivity studies,

- no minimization is required at each cell; so the efficiency and the fast computation of NN could fulfill the requirements of real-time operational applications.

The present paper is organized as follows: Section 2 is dedicated to the NN-INVERSE model and describes the methodology in details. Section 3 presents the data sets and the results obtained at the end of the inversion phase. Comparisons with existing methods are given in Section 4. Section 5 is devoted to the ambiguity removal phase and presents final maps obtained in some characteristic meteorological situations. The validity of the NN methodology is tested by running intensive comparisons that are shown in Section 6. The results are discussed in Section 7 and conclusions are presented in Section 8.

2. NN-INVERSE model

We use similar architectures as described in Thiria *et al* (1993). As mentioned above, NN-INVERSE directly gives the most probable wind vectors (aliases) from the sigma-0 measurements. An inspection of the cone like surface **(Fig. 1)** suggests that the determination of

the wind speed and azimuth results in the need to solve two distinct problems of unequal difficulty (Thiria *et al,* 1993). Due to the Lissajous ambiguities on the azimuth **(Fig. 1 b),** computing the wind azimuth is much more difficult than computing the wind speed. Since the shape and amplitude of the Lissajous curve giving the wind azimuth depends on the wind speed, (**Fig. 1 a)** the knowledge of the speed improves the determination of the azimuth. On the other hand the wind speed dependence with the azimuth seems weaker, except at very low wind speeds, which are of minor interest in meteorology and oceanography.

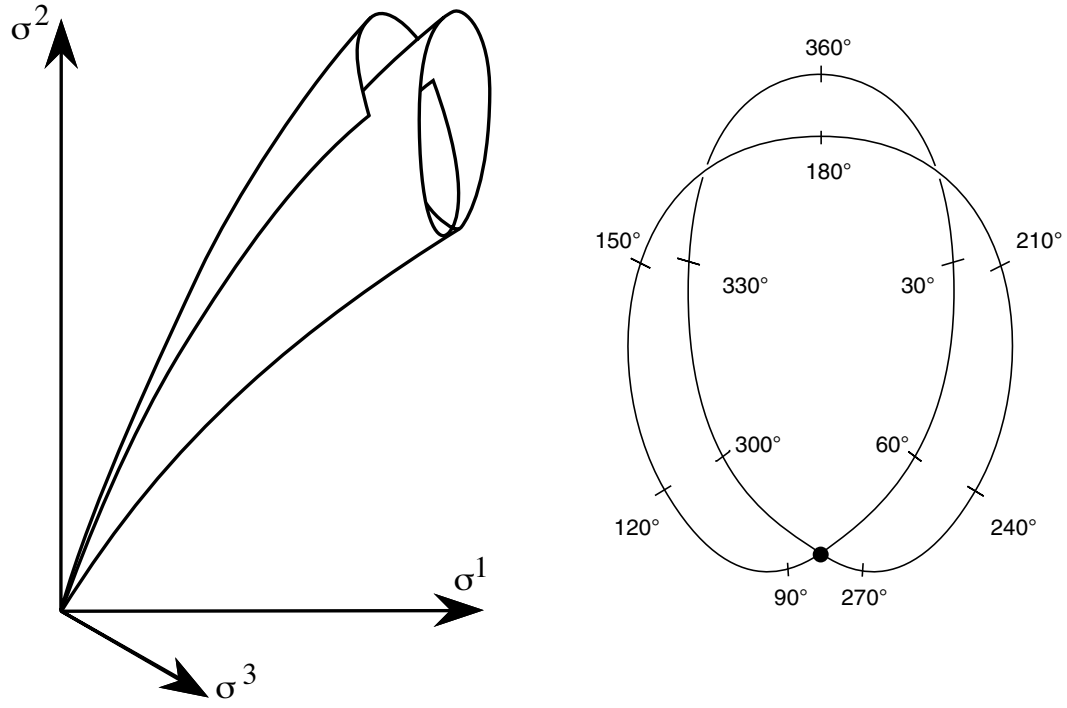

(a) **(b)**

Figure 1 : (a) Parametric representation of the ERS1 GMF in the sigma-0 space (3D). When progressing along a directrix of the cone the wind speed varies ; the different sheets of the manifold corresponds to different wind direction. (b) Graph obtained for a section at constant wind speed showing the possibility of ambiguities in the wind directions.

Since the sigma-0 measurements strongly depend on the incidence angle, the n tracks of the swath are inverted separately. The NN-INVERSE is made of n modules M_i, ($i = 1....n$) which extract the wind vector from the sigma-0 measurements. On each track i, the inverse problem has been split into two sub-problems leading to the determination of two distinct transfer functions. The first

one is a single-valued function computing the wind speed while the second one, which determines the most probable wind azimuths, is a multi-valued function. Each module consists of two levels: in the first level, a transfer function denoted as $S\text{-}NN_i$ estimates the wind speed and in the second level a second transfer function denoted as $A\text{-}NN_i$ estimates azimuth probabilities given the sigma-0 triplets and the estimated wind speed. We choose to approximate these 2**n* transfer functions of the NN-INVERSE by using multi-layer perceptrons (MLP). Such MLPs can approximate any continuous function to any degree of accuracy (Bishop, 1995). On a given level, the MLPs we used only differ by the numerical values assigned to the connection weights (parameters of NN models) which are determined during the learning phase. **Fig. 2** displays the NN-INVERSE model which is made of *n* modules M_i and a third level dedicated to the ambiguity removal. The computations of the *n* modules can be run in parallel.

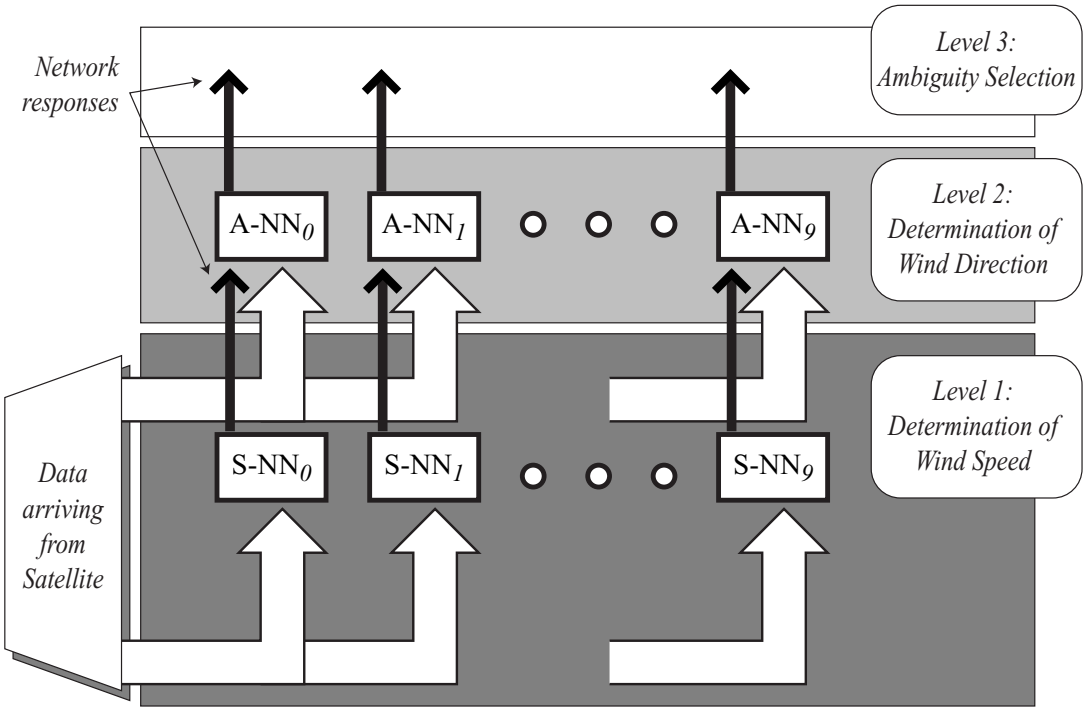

Figure 2 : Design of NN-INVERSE. NN-INVERSE is made of n different modules M_i, (n being the number of trajectories in the swath). Each module is made of a specific MLP ($S\text{-}NN_i$) estimating the wind speed and a specific MLP ($A\text{-}NN_i$) estimating the wind direction.

Sections 2.1 and 2.2 present the MLP architecture of *S-NN* and *A-NN*. Preliminary experiments using real ERS-1 (Mejia *et al*, 1994) data suggest that these architectures are adequate and have just to be optimized. In order to benefit from the information embedded in the spatial consistency of the wind field at the scatterometer scale (Thiria *et al*, 1993), the inputs of the neural networks *S-NN* and *A-NN* consist of the sigma-0 triplets corresponding to the measurements of the three antenna taken over a spatial window centered on the cell of the swath where the wind vector is determined (**Fig. 3**); this input data set is denoted as $G(\sigma_0)$. The size and the shape of the neighborhood we deal with, represents an adequate trade-off between the performance and the number of parameters to be estimated during the calibration phase (the so-called training phase).

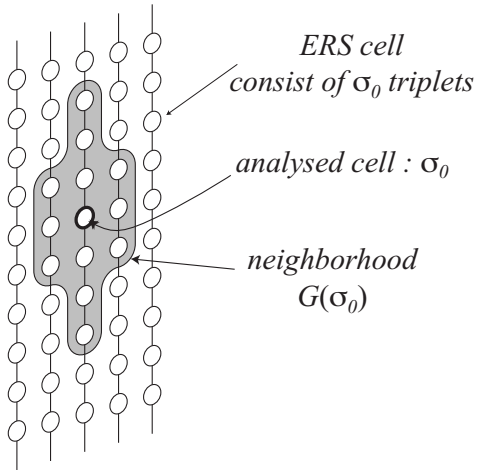

Figure 3 : Spatial context used for the determination of the wind speed and the wind direction.

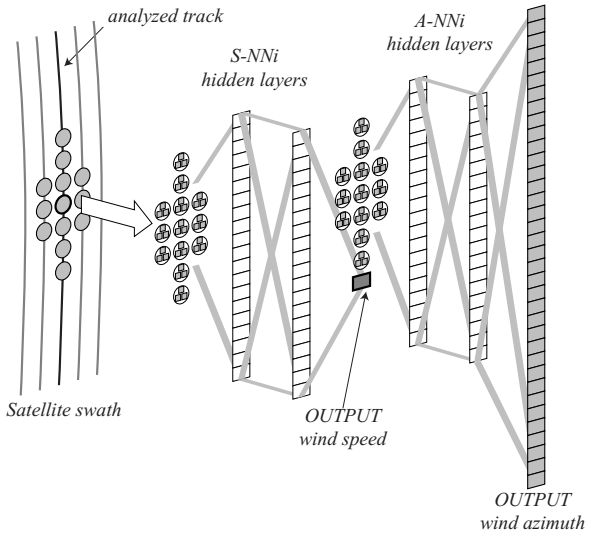

Figure 4 : Architecture of a module Mi of NN-INVERSE showing the connection between S-NNi and A-NNi.

As seen in Section 1, intrinsic errors in the most probable wind directions can remain due to the characteristics of the problem. In most cases they appear as inverted directions at ±180°. These ambiguities are removed at the third level which uses the probability of the different aliases provided by *A-NN* (Section 5).

We use sigma-0 expressed in dB which is the unit chosen by ESA for data dissemination and for a numerical reason which is to homogenize the range of the sigma-0 belonging to the different incidence angles of the spatial window.

2.1 Wind speed determination (S-NN)

S-NN$_i$ estimates the wind speed at each cell of the i^{th} track using $G(\sigma_0)$ at the corresponding point. It is a fully connected MLP with 4 layers **(Fig. 4).** The input layer is composed of 13*3 inputs which represent the 13 different triplets of the spatial window $G(\sigma_0)$. The output layer has a unique linear neuron which gives an estimate of the wind speed. The two hidden layers have 26 neurons each with sigmoidal transfer functions. Near the boundaries of the swath, adapted non-symmetric spatial windows $G(\sigma_0)$ are defined.

2.2 Wind direction determination (A-NN)

A-NN$_i$ is a fully connected MLP functioning in classifier mode **(Fig. 4).** It determines the wind direction using $G(\sigma_0)$ and the wind speed $\hat{v}$ estimated by *S-NN$_i$*. It has an input layer of 13*3+1 inputs ($G(\sigma_0)$ and $\hat{v}$) and two hidden layers of 25 neurons each. The output layer is made of 36 neurons, each neuron being dedicated to a wind azimuth interval I_{ij} of 10° such as I_{ij} = [10j, 10(j+1), j= 0, 1, ……2, 35]. As explained in (Thiria *et al*, 1993), at a given cell of the i^{th} track, *A-NN$_i$* is trained in such a way that the output approximates the posterior conditional probability density $p\left(\chi \middle| G(\sigma_0), \hat{v}\right)$, where χ represents the relative wind azimuth in degrees with respect to the scatterometer mid-beam direction. The 36 outputs of *A-NN$_i$* display a discrete approximation of $p(\chi | G(\sigma_0), \hat{v})$. The four most probable wind azimuths (aliases) are given by the azimuths associated to the I_{ij} having the highest posterior probability. Each alias is determined with an

accuracy of ±15° by computing the expected value of 3 adjacent intervals and combining them as shown in the study of Thiria *et al* (1993).

The $S\text{-}NN_i$ and $A\text{-}NN_i$ have 1405 and 2616 parameters that are respectively estimated from a learning set. These parameters are determined by minimizing a quadratic cost function of the form:

$$C(W) = \sum_k |S_k - Y_k|^2$$

where S_k represents the output computed by the MLP and Y_k the desired output provided by the corresponding data set, the summation being taken over the dedicated learning set.

For both MLPs this cost function is the most appropriate:

For $S\text{-}NN_i$ which is a regression function, taking into account the output and input noises is important (Stoffelen and Anderson 1997a). The variance of the wind speed error is globally known (its standard deviation is 1.5 ms^{-1}, Stoffelen and Anderson 1997b) but there is no information on the local error variance at a given wind speed. In this case the use of the Maximum Likelihood (MLE) cost function as defined in Stoffelen and Anderson (1997a) will bring no improvement. Taking into account the scatterometer errors is not easy since it would be necessary to model the sigma-0 variance. Moreover as we have chosen to work in dB, a MLE cost function is not valid since the noise of the signal is not Gaussian (Rufenach, 1998, Stoffelen and Anderson, 1997b).

For $A\text{-}NN_i$, the simple quadratic function implies we obtain an approximation of posterior probabilities (Richard and Lippman 1991).This cost function choice has also proven to be efficient in the ambiguity removal phase.

The minimization is performed by using a stochastic gradient descent algorithm. This modeling phase is done once for each MLP. When using NN-INVERSE, wind parameters are directly computed by applying the associated MLP functions to sigma-0 observations.

3. The data set

The parameters of the different MLP of NN-INVERSE model were computed using ERS-1 scatterometer sigma-0 collocated with ECMWF wind vectors interpolated by CERSAT/IFREMER (I-ECMWF hereafter). The data period extends from July 1994 to April 1996 onto the North Atlantic Ocean, (100W, 5W) to (60N, 20 N).

We used the data provided by CERSAT/IFREMER without any specific quality test on the wind vectors; we checked the quality of the signal according to ESA/UWI requirements. The North Atlantic ECMWF winds are thought to be of good quality owing to the relatively high density of observations which are assimilated in the numerical model. The overall data set used consists of approximately 390000 collocated pairs (sigma-0, interpolated ECMWF wind vectors) for each track.

The accuracy of the inversion greatly depends on the distribution of the learning data set (LEARN hereafter). Taking LEARN at random gives rise to the usual distribution of the wind vectors which is centered at around 7 ms^{-1} leading to a very accurate determination of the most usual wind speeds in the range ($4m/s < v < 14m/s$) and less accurate outside that range. Such a learning data set leads to a substantial drop in accuracy when retrieving high wind speeds ($v > 18m/s$) which are of importance in oceanography and meteorology. A way to overcome this drawback is to take a uniform distribution that equally represents all speeds and directions in order to get a statistically representative data set without increasing biases. For each MLP, LEARN is made of about 24000 pairs $\{G((\sigma_0), (v,\chi))\}$, where (v,χ) represents the speed and the

azimuth of wind at the center of the spatial window. The distribution we use is quasi uniform for wind vectors in the domain [0°,360°]x[3.5 m/s, 25 m/s]. In order to test the performances of NN-INVERSE we built a test set having the same characteristics and presenting a quasi uniform distribution in the same range ([0°,360°]x[3.5 m/s, 25 m/s]); we will denote it as QU-TEST hereafter. For each MLP, QU-TEST is made of 5000 pairs taken at random from the data which have not been used for LEARN. **Fig. 5 a** and **b** show the histograms of the data distributions used for LEARN and QU-TEST for M_4 (NN-INVERSE for mid-swath track). There are some faults in the sampling; high wind speeds above 18m/s are under represented leading to less accurate high wind speed retrieval. In order to test NN-INVERSE for actual wind vectors we use another test set made of 322 swaths of collocated ERS1 sigma-0 and I-ECMWF Wind fields observed in May 1996 which have not been used in learning; this test set is denoted as S-TEST. We added several swaths to it taken in 1994 and 1995, that contain more complex meteorological situations like deep lows and fronts.

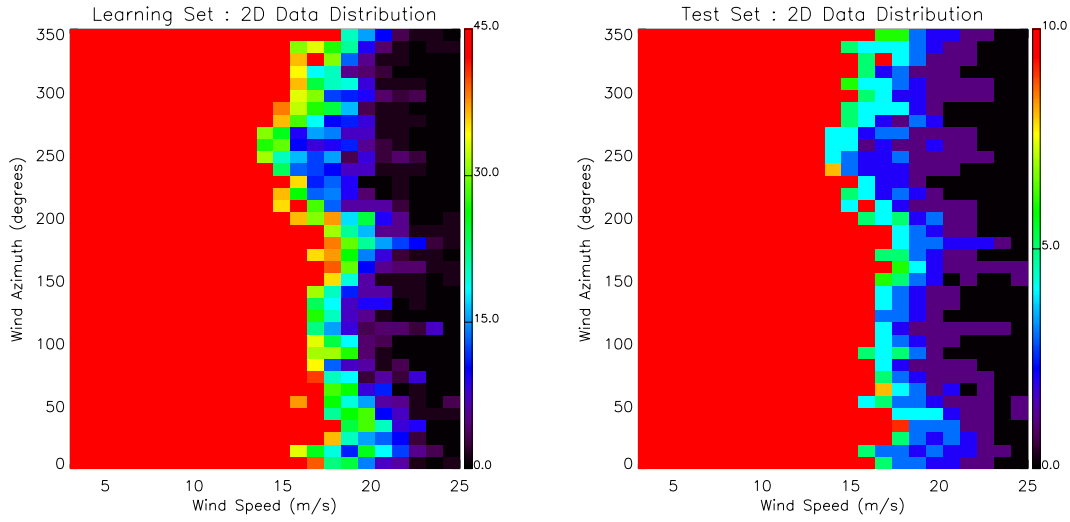

(a) **(b)**

Figure 5 : Two dimensional data distribution with respect to wind speed and wind direction for LEARN (a) and QU-TEST (b) for the 4th track.

S-TEST contains about 100000 wind vectors with speeds ranging from 4.0 m/s up to 26.0 m/s. Inverting a whole swath allows us to examine the correlation of the errors and to compare the

quality of the retrieved wind fields (after the removal of ambiguities) with other operational products.

4 - Performances of NN-INVERSE before disambiguation

We now present statistical tests to evaluate the accuracy of the NN-INVERSE model against I-ECMWF winds before removing the ambiguities. These tests are independent of any errors due to bad selection of aliases in the ambiguity removal procedure.

track	0	1	2	3	4	5	6	7	8	9
bias (m/s)	-0.2	0.0	-0.1	-0.1	-0.1	-0.1	-0.1	-0.1	0.0	0.0
RMS(m/s)	1.6	1.6	1.5	1.6	1.6	1.6	1.6	1.6	1.6	1.7

Table 1 : Performances of NN-INVERSE when approximating the wind speed : the first row gives the bias with respect to the track and the second gives the RMS.

Track nb of alias	0	1	2	3	4	5	6	7	8	9
1	78.4	77.9	79.3	79.5	78.1	73.1	73.7	65.9	71.4	66.3
1+2	85.1	85.0	86.9	87.7	87.5	87.8	87.6	88.0	88.2	86.9
1+2+3	86.1	85.9	87.6	88.6	88.4	88.8	88.4	88.8	88.8	87.6
1+2+3+4	86.5	86.4	88.0	89.0	88.7	89.1	88.7	89.1	89.1	87.9

Table 2 : Performances of NN-INVERSE for wind direction retrieval against I-ECMWF. Each row displays the performances reached by A-NN_i, for each track i and for the most probable solution (first alias denoted as "1"), the first plus the second alias (denoted as "1+2"), the first plus the second plus the third alias (denoted as "1+2+3"), the first plus the second plus the third plus the fourth alias (denoted as "1+2+3+4"). A given direction is considered correct if the computed direction differs by less than ±20° from the I-ECMWF direction.

We used the QU-TEST, which allows us to consider the errors for an homogenized data set. We give the performances for each track and for each MLP (*S-NN* and *A-NN*) separately. **Tab. 1** gives

the results for the ten *S-NN*$_i$ and **Tab. 2** the results for *A-NN*$_i$. The detailed description of the statistical estimators is given in **Appendix 1**.

Tab. 1 shows that the bias and the RMS of the wind speed are very low and not dependent on the track, which proves the good quality and the homogeneity of NN-INVERSE since each track is inverted by using a specific NN model.

The results of **Tab. 2** show that :

- the good quality of the first rank solution; the first alias (the wind direction having the highest probability and presented in row 1 of **Tab. 2**) given by the NN-INVERSE matches the I-ECMWF direction ±20° in 75% of collocations, which is a dramatic improvement with respect to usual methods whose skill is about 60% (Rufenach, 1998, Stoffelen, personal communication). The skill of the first and second alias (presented in row 2 of **Tab. 2**) is 87%.

- the existence of a good solution among all the four aliases; about 88 % of the directions are consistent with I-ECMWF. For the remaining 12 % we can not state the error sources without further investigation since I-ECMWF is not an error-free reference.

These good performances are mainly due the spatial context used in the input of the *S-NN* and *A-NN* and to the overall neural networks abilities to model non-linear phenomena.

5. Ambiguity removal

The problem consists in finding the best physical solution in a large combinatorial space. This space is made of all the wind fields which are solutions with their multiple aliases. Considering the two first aliases only and a 1000-km long swath, this space contains more than 10^{60} possible wind fields. Assuming that the accuracy of the inversion is sufficiently good (i.e. it exists a solution close to the true field in this space), then removing the ambiguities consists of finding the

most physically consistent wind field that corresponds to the true wind field. This is a very complex problem for the following reasons:

- it is difficult to assess the physical consistency of a meteorological wind field in a simple and fast way,

- due to the size of the combinatorial space, the search of a solution is a critical operation,

- more than one consistent field may exist; as an example two acceptable uniform wind fields differing by 180° could be found, but only one of the two corresponds to the true solution.

The last two points address the importance of the first rank solution (most probable wind vector) provided by the inversion; the closer this solution to the truth, the more easily the problem is solved. Usually the ambiguity removal algorithms (CREO, PRESCAT) solve this problem by using a reference wind field provided by a NWP model in order to select the closest wind field in the solution space as a start-field. Obviously, this may lead to some errors in the wind selection since the prediction of NWP models could be far from the truth, particularly in locating accurately the wind structures (front, lows, ...) over the oceans.

The ambiguity removal is performed using an adapted version of PRESCAT denoted as PRESCAT-NN hereafter. The PRESCAT algorithm was originally developed by Stoffelen (Stoffelen and Anderson, 1997c) and appears to be the most skillful wind ambiguity removal procedure (Stoffelen and Anderson, 1997c) at the present time. This algorithm requires a first guess wind field provided by a NWP model. In PRESCAT-NN, we select the different solutions using a trade-off between the closest NN-INVERSE aliases to the direction of ECMWF model and their probabilities given by NN-INVERSE. The resulting wind field is denoted as the start-field. If the probability of the first alias given by NN-INVERSE is high, then priority is given to it. If not, the chosen alias is determined by computing a normalized distance between the different vectors provided by NN-INVERSE and the ECMWF model wind vector weighted by the posterior probabilities of the different alias. The chosen alias corresponds to the minimum of this

distance. The resulting start-field could be very different from the ECMWF model wind field unlike to PRESCAT. For each chosen vector of the start-field, we compute a confidence coefficient which is a composite number taking into account the different probabilities provided by NN-INVERSE and the different distances to ECMWF model wind direction.

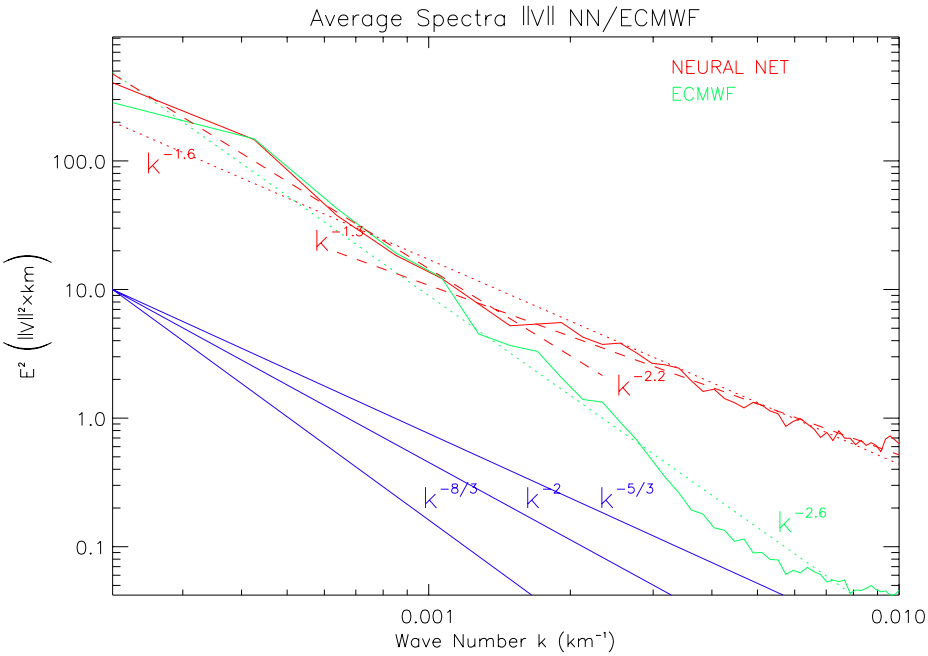

Figure 6 : Along track wind kinetic energy spectrum averaged on 40 tracks (4 swaths) with respect to the wave number; the red color corresponds to neural networks winds while the green to ECMWF winds. In full line, we have drawn some theoretical spectrum slopes showing that the different wind spectrum are close to those of classical geophysical turbulence theories.

Then this start field is iteratively smoothed by a 3X3 (150 km x 150 km) spatial filter which chooses the alias in the center of the window that minimizes the global wind variance in the spatial window. The weights of the spatial filter are initialized with the confidence coefficients coming from the first step and are updated at each iteration as described in the initial Stoffelen and Anderson (1995) method.

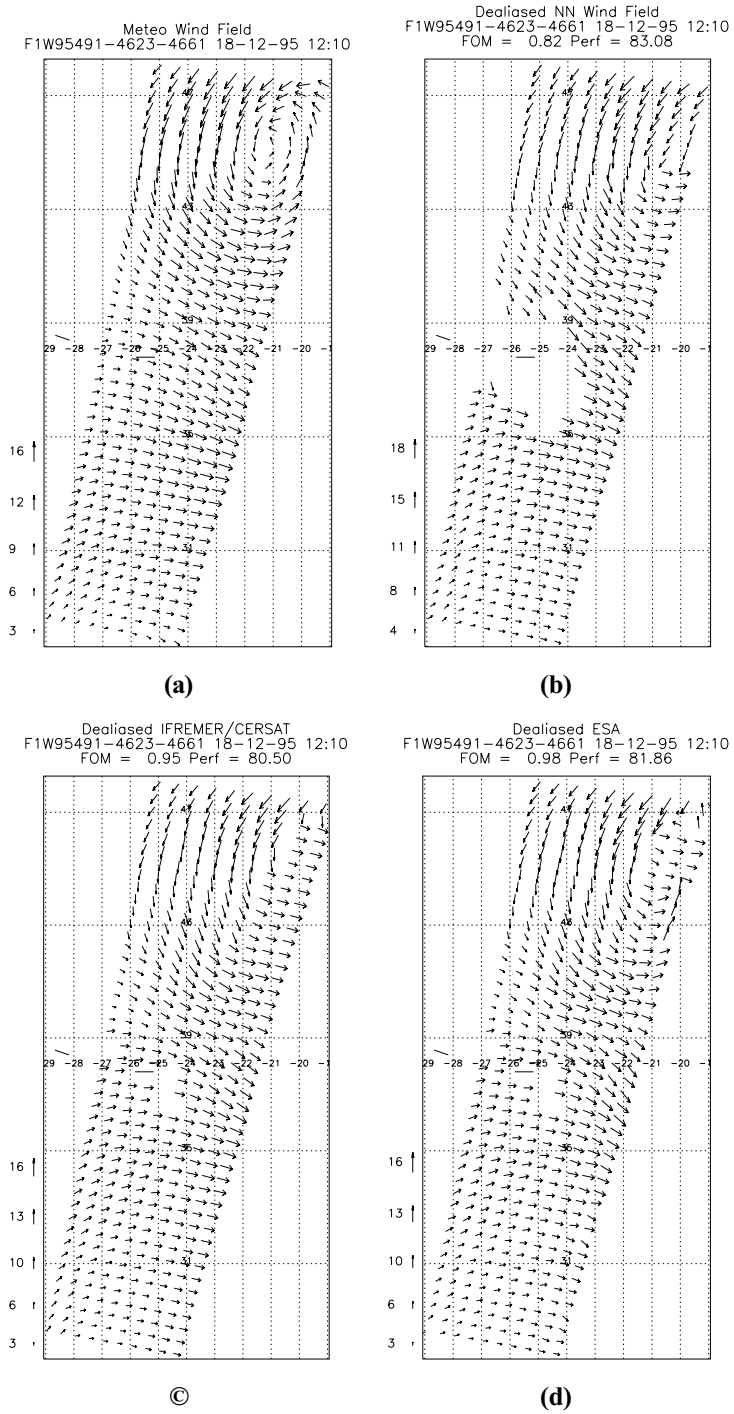

Figure 7 : Example of wind field maps : (a) I-ECMWF (b) NN-INVERSE, (c). CERSAT, (d) ESA. This example shows the importance that ERS1 scatterometer wind field could have brought to NWP models in this situation. The forecasted low in the NE corner is seen eastward and outside of the swath by all the inverse methods.

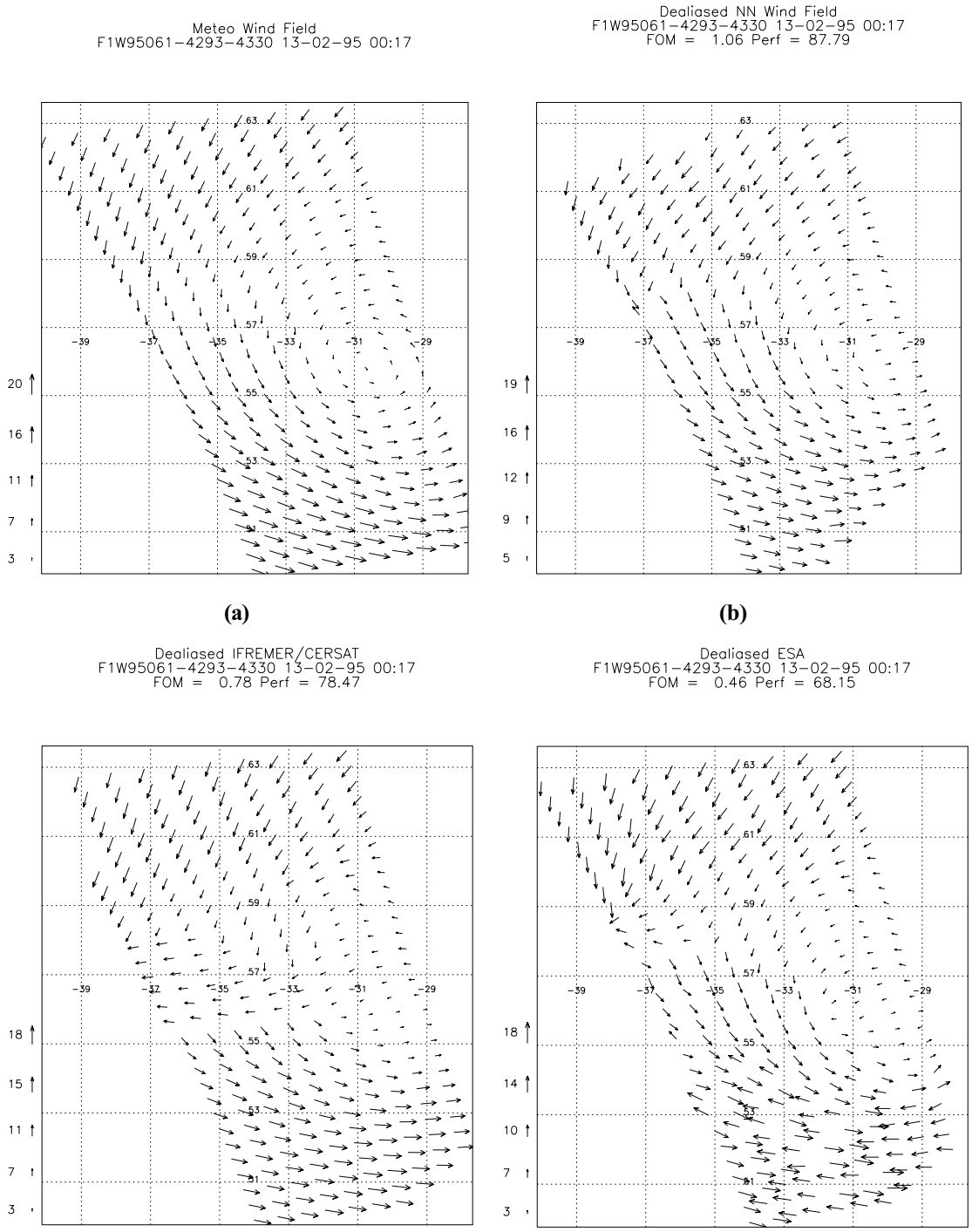

Figure 8 : Example of wind field maps : (a) I-ECMWF (b) NN-INVERSE, (c). CERSAT, (d) ESA..

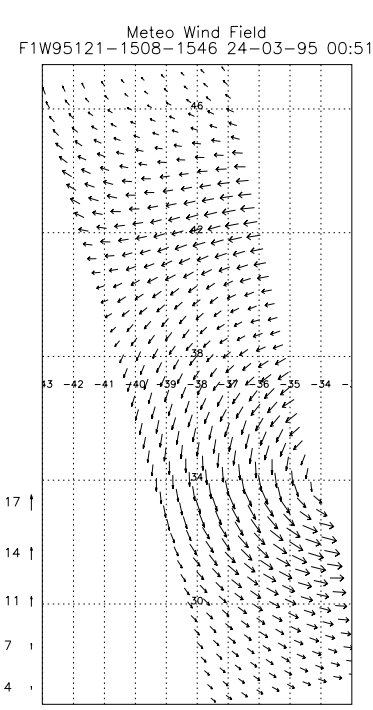

(a)

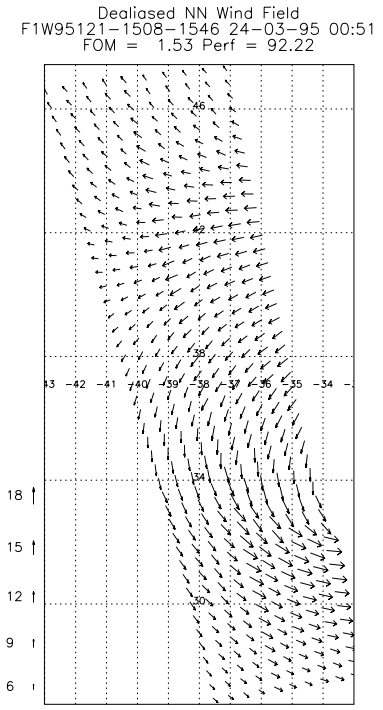

(b)

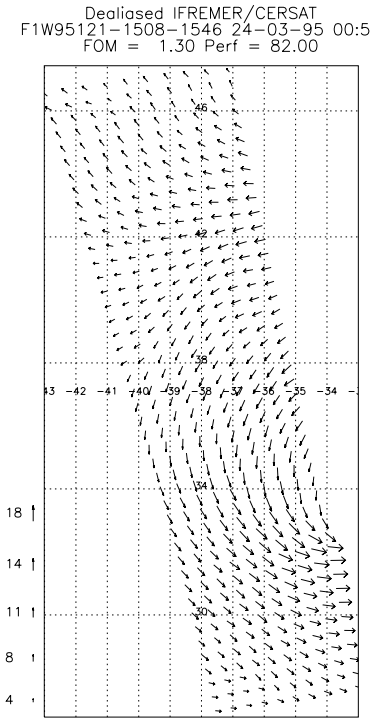

(c)

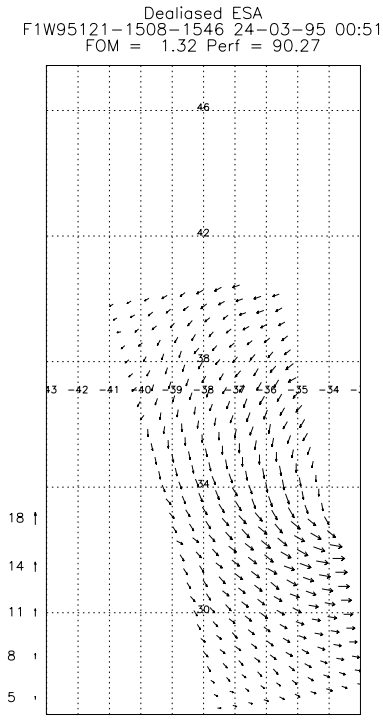

(d)

Figure 9 : Example of wind field maps (a) I-ECMWF (b) NN-INVERSE, (c). CERSAT, (d) ESA.

Fig. 7-b, **8-b** and **9-b** are examples of final wind fields; first NN-INVERSE has been applied on ERS data to retrieve a set of wind solutions, then PRESCAT-NN has been applied to remove the ambiguities among the multiple aliases. In order to evaluate the quality of the retrieved wind fields, we have computed the one dimensional wave number spectrum for both the neural methodology (after disambiguation) and the ECMWF wind fields (**Fig. 6**). It can be seen that the neural methodology spectrum is more energetic at high wave numbers than ECMWF spectrum, showing the ability of scatterometer winds to capture small-scale features. We can not state firmly, without further investigation, that this increase of energy at high wave number was not partly due to white noise colored by the non-linear processing of the neural networks. Nevertheless, we can remark the consistency between the slope at high wave numbers and some expected theoretical spectra (in blue lines) at these scales. Unfortunately the spatial averaging used in the wind vector computation may filter some of small-scale structures in the wind field. But we think it is better to increase the performance of the wind retrieval by using a spatial filter even if we loose small scale features rather than introduce noise in the difficult attempt to keep these small scale features.

6. Performances after Disambiguation and Comparisons with other Methods

We checked the performances of NN-INVERSE after the disambiguation phase and compared them to those of ESA and CERSAT/IFREMER wind products on the S-TEST data set. This set contains the wind vectors given by PRESCAT-NN and the dealiased wind vectors distributed by CERSAT and by ESA. ESA wind retrieval is based on the CMOD4 GMF (Stoffelen 1995, Stoffelen and Anderson 1997a) and CERSAT/IFREMER is based on the CMOD-IFR2 GMF (Quilfen and Bentamy, 1994).

In these comparisons we use exactly the same data for the three methods. When one of the methods does not provide a solution for a given signal the associated wind vectors of the two

others are also removed from the test. As a consequence S-TEST shrinks from 100000 to about 71000 comparable winds. Because this reduction is essentially due to the ESA quality control and occasionally to the IFREMER one, the performances would be biased in favor of ESA and IFREMER.

Data Set 71436 data	**S-TEST True Distribution**			**S-TEST Mean Bin Average**		
inverse model	**NN-INVERSE**	CERSAT	ESA	**NN-INVERSE**	CERSAT	ESA
Speed Bias in m/s	0.2	**-0.1**	-0.8	**-0.5**	-1.26	-2.1
Speed Stdv in m/s	**1.4**	1.5	1.5	1.7	***1.6***	***1.6***
Dir Bias in degree	-0.2	**-0.0**	-0.4	**-0.1**	-0.5	1.0
Dir Stdv in degree	**17.8**	26.9	42.9	**16.3**	21.5	43.7
Vector Bias in m/s	**0.2**	0.4	0.5	**0.8**	1.4	2.1
Vector Stdv in m/s	**2.8**	3.6	5.1	**3.6**	4.1	7.2
Perf @ 20° in %	**91.1**	84.6	81.0	**92.3**	88.1	83.6

Table 3.1 : Performances of the different inversion methods on S-TEST ; in **italic bold** performances when they are equivalent (difference between the performances less than 5%), in **bold** the best performances (difference between the performances between 5% and 10%), **in bold and underlined** the performances which are the highest (higher than 10 %).

I-ECMWF speed in m/s	< 4	4 - 8	8 - 12	12 - 16	16 - 20	> 20
% of S-TEST	6.46	51.79	29.84	9.37	2.08	0.47

Table 3.2 : distribution in % of the data used in **Tab. 3.1** on the bins. The shaded column is only given for information, those winds (speed less than 4 m/s) are not used in statistics.

We also checked the accuracy of the different inversion methods independently of ambiguity removal. For this purpose as suggested by Stoffelen and Anderson (1997b), we use a subset of S-

TEST, denoted as S90-TEST. The S90-TEST data set only contains data where the wind direction of the three products is pointing in the same half plane as defined by the I-ECMWF wind. If one product selects an ambiguous direction, the corresponding three products will be thrown out from the S90-TEST database. We thus reject data with possible ambiguous direction at 180° from S90-TEST. It would have been better to find the closest alias direction among all possible directions, as done in Section 4 but this was not possible since ESA UWI product does not provide the different wind solutions, only the dealiased one.

Data Set 69133 data	**S90-TEST True Distribution**			**S90-TEST Mean Bin Average**		
inverse model	**NN-INVERSE**	CERSAT	ESA	**NN-INVERSE**	CERSAT	ESA
Speed Bias in m/s	***0.1***	***-0.1***	-0.8	**-0.7**	-1.3	-2.1
Speed Stdv in m/s	**1.3**	1.4	1.5	1.6	**1.5**	1.6
Dir Bias in degree	**-0.7**	-0.9	-0.6	**-0.3**	-1.2	0.8
Dir Stdv in degree	**12.9**	15.2	40.0	**12.1**	13.4	42.2
Vector Bias in m/s	**0.2**	0.3	0.5	**0.8**	1.3	2.1
Vector Stdv in m/s	**2.3**	2.6	4.8	**3.1**	3.3	7.0
Perf @ 20° in %	**91.4**	86.6	82.2	***92.6***	***89.4***	84.3

Table 4.1 : Performances of the different inversion methods on S90-TEST ; in ***italic bold*** performances when they are equivalent (difference between the performances less than 5%), in **bold** the best performances (difference between the performances between 5% and 10%), **in bold and underlined** the performances which are the highest (higher than 10 %).

Tab. 3.1 (**Tab. 4.1)** gives the bias and the standard deviation for the wind speed error, the wind direction error, the wind vector error and the percentage of agreement with I-ECMWF wind direction at ±20° (denoted as Perf at @ 20° in the tables) for S-TEST (S90-TEST). The definition of these statistical parameters is given in **Appendix 1**. The three first columns show the

performances computed on the true distribution of S-TEST (S90-TEST). In the three last ones performances are computed as follows: we first considered five bins of wind speed and separately compute the performances in each bin, later we averaged these performances in order to give the same weight to each wind speed interval. **Tab. 3.2** (**Tab. 4.2)** displays the distribution in % of the data over these bins for S-TEST (S90-TEST).

I-ECMWF speed in m/s	< 4	4 - 8	8 - 12	12 - 16	16 - 20	> 20
% of S90-TEST	6.00	51.83	30.14	9.41	2.13	0.49

Table 4.2 : distribution in % of the data used in **Tab. 4.1** on the bins. The shaded column is only given for information, those winds (speed less than 4 m/s) are not used in statistics.

Tab. 3.1 shows that the neural methodology compares well with the others methods. The standard deviation for the wind speed and wind direction fit the ESA specifications which are ±2m/s and ±20°. In addition, we remark that the mean bin average performances of the neural methodology are less deteriorated than others, stressing the importance of the quasi-uniform distribution used during training. In this case, the standard deviation of wind direction and Perf @ 20° also improve showing that at high wind speed the retrieval of wind direction is good.

Comparing **Tab. 3.1** with **Tab. 4.1** shows that there is a small increase in general performance but NN-INVERSE still appears better than the two others. This is due to the accuracy of the first rank solution of NN-INVERSE that gives considerable help to the ambiguity removal. For the CERSAT product, the increase in performance is very clear. The good overall score suggests that CMOD-IFR2 is quite an accurate GMF but that the ambiguity removal scheme is weak. Moreover this could also be explained by the advantage of using a spatial context rather than a one cell inversion. Whatever the accuracy of inversion and the skill of the ambiguity removal are, it will not be possible to retrieve a good wind field if there are not sufficient well oriented winds (first rank alias).

Fig. 7, **8** and **9** display three distinct wind fields retrieved using NN-methodology and the other methods. We see that all the retrieved wind fields are very consistent (small divergence and no abnormal fronts). When compared to I-ECMWF wind fields it is seen that the shape and the center of meteorological perturbations are slightly modified showing the ability of the scatterometer to exactly map the instantaneous wind field. In **Fig. 7**, the forecast low in the NE corner is seen eastward and outside of the swath by all the inverse methods. The NWP model is probably wrong as shown by the high consistency between the three inverse methods. In the center of the swath we notice the only drawback due to the use of a spatial context; the gaps due to unusable or missing ERS data increase in size because all data in $G(\sigma_0)$ must be usable. In **Fig. 8** we can note many differences between the methods. For this situation, NN-INVERSE and PRESCAT-NN produce an outstanding wind field in comparison with the other methods. In **Fig. 9** the I-ECMWF wind field is quite homogeneous and seems to be close to the measured scatterometer winds. It results in a good agreement and a successful removal of ambiguities for all inverse methods. Nevertheless, these inverted wind fields present some differences in shape and speeds.

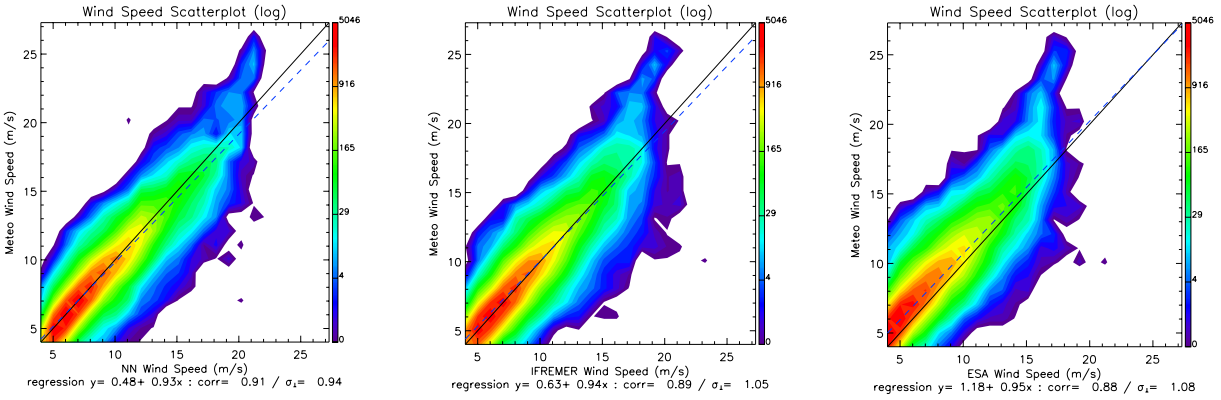

(a) **(b)** **(c)**

Figure 10 : wind speed scatterplots, I-ECMWF wind speed (ordinate) vs. scatterometer wind speed (abscissa) for (a) NN-INVERSE, (b) CERSAT and (c) ESA.

In order to test the consistency of the different inversion methods with respect to NWP models, we display different scatter plots computed by using the S-TEST data set. For all of them we

also give the parameters of a linear regression of the cloud, the correlation factor and $\sigma_\perp$ which is the standard deviation orthogonal to the linear regression line.

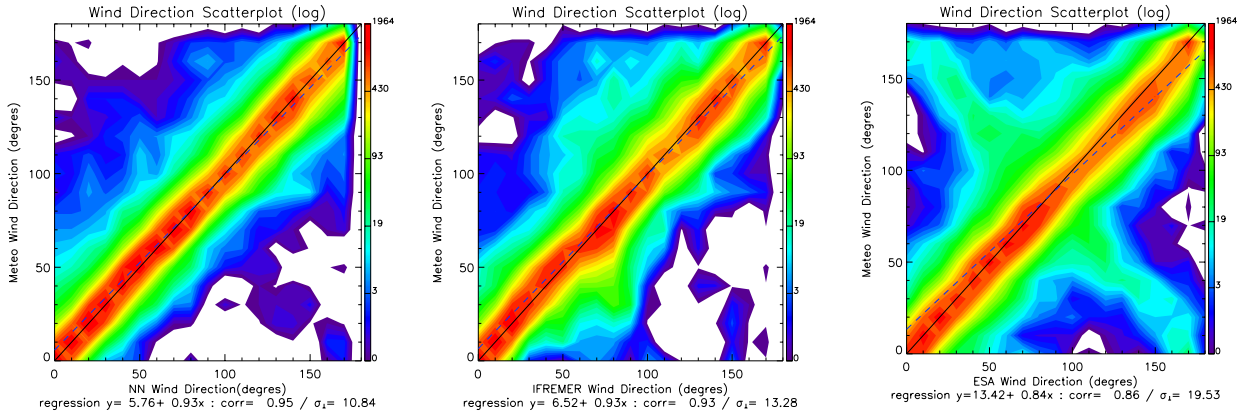

(a) **(b)** **(c)**

Figure 11 : wind direction scatterplots : I-ECMWF wind direction (ordinate) vs. scatterometer wind direction (abscissa) for (a) NN-INVERSE, (b) CERSAT and (c) ESA.

Fig. 10 a, b and **c** display scatterplots for the retrieved wind speed with respect to the I-ECMWF wind field for the three methods. High winds are underestimated by all three methods. **Fig. 11 a, b** and **c** show the scatterplots for the wind direction (after disambiguation) with respect to I-ECMWF wind fields for the three methods.

The different statistical estimators computed from the scatter plots (linear regression, correlation coefficient) show that the neural methodology has a good skill when compared to the two other methods.

We also computed the scatter plots for each wind components with respect to ECMWF wind fields (**Fig. 12 a, b** and **c**). This allows us to check the consistency of the retrieved wind vector. One can still notice the influence of remaining wind ambiguities on the ESA and CERSAT scatterplots appearing as abnormal scatters along the second diagonal.

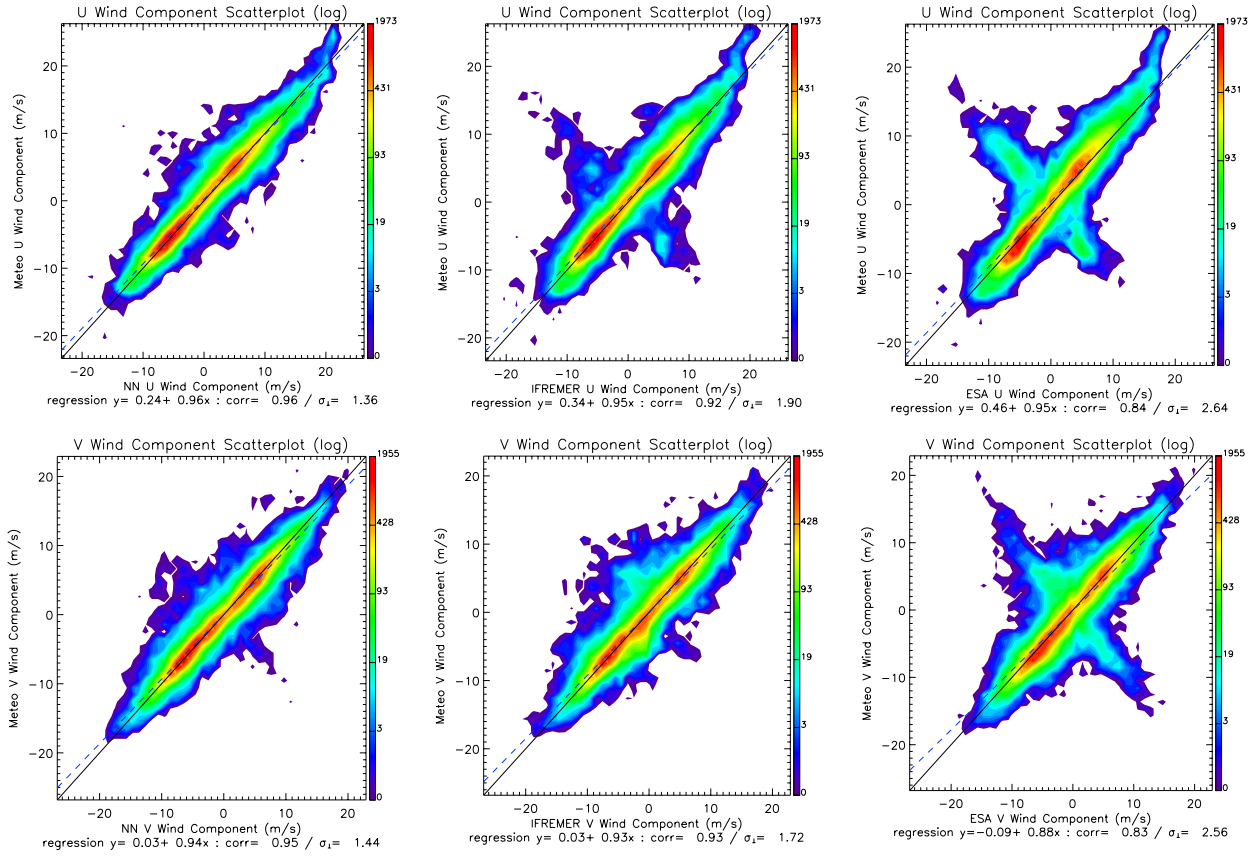

(a) **(b)** **(c)**

Figure 12 : wind components (u,v) scatterplots, I-ECMWF wind speed (ordinate) vs. scatterometer wind speed (abscissa) for (a) NN-INVERSE, (b) CERSAT and (c) ESA.

In **Fig. 13 a, b** we present the histograms for the speed (**a**) and the direction (**b**) of the retrieved winds for the three methods. These histograms are close together and to that of ECMWF showing the good quality of the wind retrieval algorithms except for ESA at low wind speeds.

In Fig. 14 we display the histograms for the two components of the wind. It is seen that these two-dimensional histograms are quite homogeneous and are in good agreement with this of I-ECWMF. The large hole in the center of these histograms is due to the fact low wind speeds (under 4 m/s) are not included in S-TEST.

In order to compare the performances of the different models, a number (the so-called Figure Of Merit or FoM, see **Appendix 2** for the definition) has been proposed by Offiler (1994). The

greater FoM, the better the inverted wind field. A FoM of 1 indicates that ESA specifications of ±2m/s and ±20° are fulfilled.

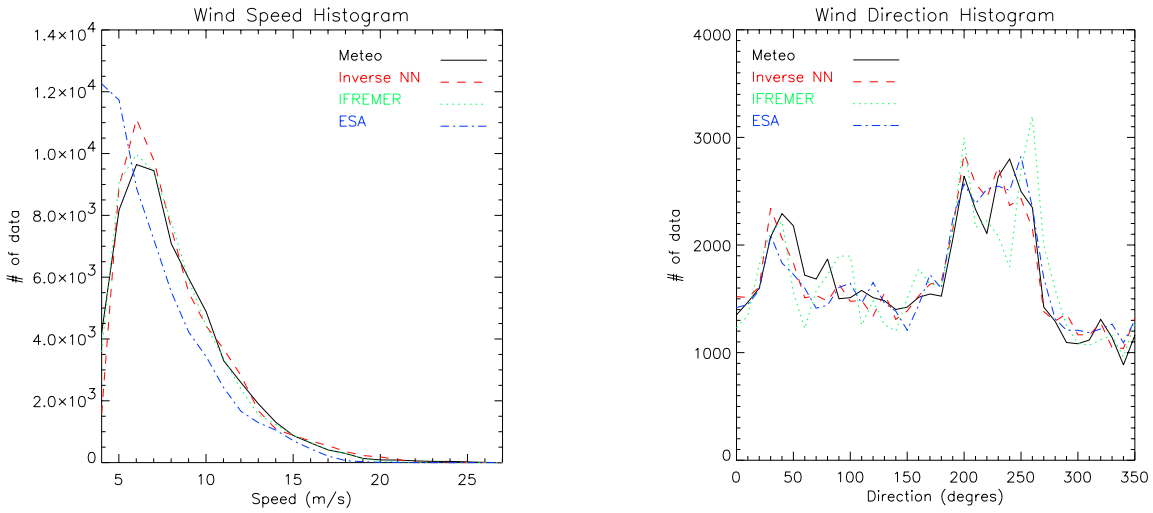

(a) **(b)**

Figure 13 : wind speed histogram (a) and wind direction histogram (b) for I-ECMWF (black solid), NN-INVERSE (red dash), CERSAT (green dot) and ESA (blue dash-dot).

speed m/s	true	<4	4 - 8	8 - 12	12 - 16	16 - 20	>20	mean
NN-INVERSE	**1.29**	**1.15**	**1.55**	**1.23**	**1.04**	**1.00**	**1.03**	**1.17**
CERSAT	1.05	1.05	1.23	1.05	0.81	1.00	1.01	1.02
ESA	0.76	0.88	1.01	0.72	0.58	0.54	0.43	0.67

Table 5 : FoM for S-SET with respect to the wind speed and for the true distribution of S-TEST and averaged over each bins. The shaded column gives the FoM for winds speed less than 4 m/s and is given only for information, those winds are not used for computing the FoM for true distribution and bin average.

We compute FoM for the three different inverse methods on S-TEST; **Tab. 5** presents the results with respect to different I-ECMWF wind speed ranges. We also give the FoM for the true distribution of S-TEST and the normalized one given by the mean of the FoM over each bins.

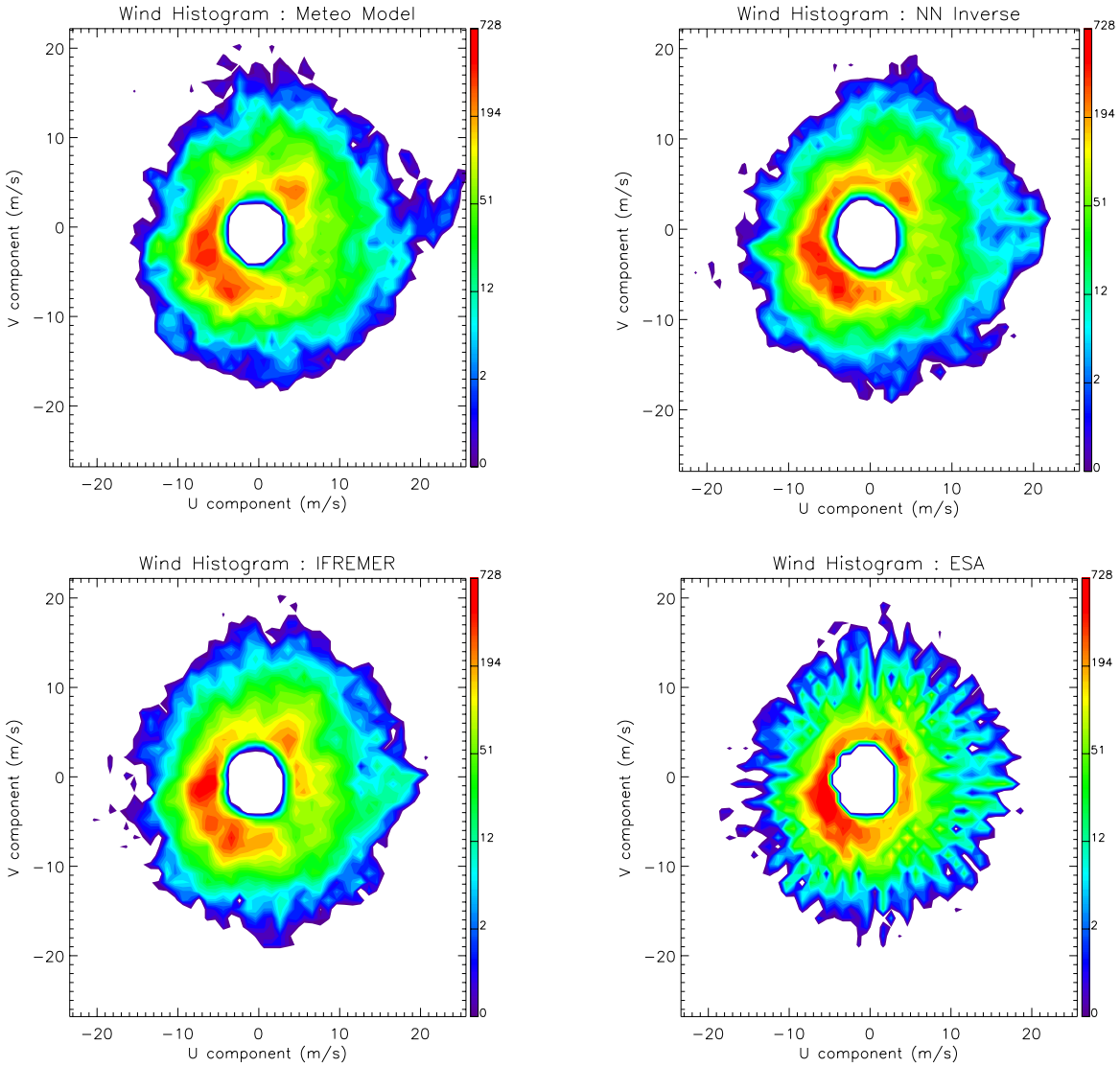

(a) **(b)**

Figure 14 : 2D wind histogram in (u,v) component space, I-ECMWF (a), for NN-INVERSE (b), CERSAT (c) and ESA (d).

Once again neural methodology appears the most skilful model either for true distribution or for the normalized one.

7-Discussion

NN-INVERSE produces a skill of 75% for rank1 ambiguity which is better than the skills of the other methods which are around 60% (Rufenach, 1998, Stoffelen, personal communication). This good performance is mainly due to the ability of NN-INVERSE to use a spatial context which adds valuable information with respect to a single sigma-0 triplet. The spatial context processing differs from a simple spatial filtering in the sense that it is intrinsically embedded in the NN-INVERSE functioning. A tentative physical interpretation is the following: the cones corresponding to the different cells of the spatial window are different and the position of each sigma-0 triplet of the spatial window with respect to each cone is different in the sense that some of them might be out of the ambiguity region contributing significantly to a correct estimation of the first alias.

The good skill of NN-INVERSE when compared to ESA and IFREMER procedure is confirmed on tests done using the S90-TEST database.

The PRESCAT NN takes into account the posterior probabilities on the wind direction given by NN-INVERSE to remove the ambiguities. The good performance of the NN retrieved wind are thus due to the combination of NN-INVERSE and PRESCAT-NN. As in every methodological comparison, bias may be introduced due to the fact that the CMOD4 GMF (ESA GMF) and CMOD2-I3 (IFREMER GMF) used for the inversion, have been calibrated using ECMWF output during 1992-1993. Since this period, the quality of ECMWF winds has dramatically improved leading to a bias in the comparison with the NN method which has been trained using data from July 1994 to April 1996.

All three methods yield poor performance when retrieving the wind direction at low wind speed. **Tab. 6** compares the statistics on wind direction computed for S-TEST true distribution with S-TEST true distribution extended to wind with speed less than 4 m/s. Although such winds represent only 6.5 % of the data, their impact on wind direction RMS error and thus Perf @ 20°

is significantly obvious. The three methods increase their RMS error on wind direction by 2.1° for NN-INVERSE, 1.7° for CERSAT and 3.6° for ESA. They decrease Perf @ 20° by 2.1 %, 2.6 % and 3.6 % respectively. Since all methods show this deficiency it seems that this phenomenon is due to an intrinsic limitation of the physics of the scatterometer rather than to a modelling deficiency. We suggest that the development of the surface ripple waves under low wind is not sufficient to ensure an accurate estimation of wind direction. For this reason, we recommend very careful use of scatterometer winds when their speed is less than 4 m/s.

Model	NN-INVERSE		CERSAT		ESA	
Error measure	Dir RMS	Perf @ 20°	Dir RMS	Perf @ 20°	Dir RMS	Perf @ 20°
S-TEST + 4 m/s	19.9°	88.9 %	28.6°	82.0 %	46.5°	77.4 %
S-TEST	17.8°	91.0 %	26.9°	84.6 %	42.9°	81.0 %

Table 6 : Impact of winds at low speed (< 4 m/s) on the RMS direction error and Perf @ 20° computed on S-TEST true wind distribution. "S-TEST + 4 m/s" contains the winds of S-TEST extended to winds with speed less than 4 m/s.

Obviously the use of a spatial context gives directional information that explains the good skill of the first rank solution and consequently the high quality of the final wind fields after ambiguity removal. The main drawback is that all 13x3 sigma-0 must be used in the input; the area containing unusable ERS measurements increase in size in comparison with the one-cell inversion. This impact can be seen in the middle swath of **Fig. 7-b**. Such a spatial context could also introduce a possible spatial filtering on the wind field. Besides since we used a NWP to train the relationships between the wind and ERS signal, it may result a loss of geophysical variance at the lowest spatial scales.

8-Conclusion

This paper presents a neural networks methodology to retrieve the wind vector from ERS1 scatterometer data. The inversion of the scatterometer data is complex since the sigma-0 triplets can lay in regions of the sigma-0 space where the direction is intrinsically ambiguous as explained in the introduction. NN-INVERSE provides an estimate of the posterior probability of the different alias for the wind direction. The most probable wind direction (rank 1 solution) given by NN-INVERSE has a skill of 75% while those of the other methods is of about 60%. This clearly shows the improvement of NN-INVERSE with respect to the other methods. The remaining ambiguities are then removed by an adapted version of the PRESCAT algorithm which uses a meteorological wind field provided by a NWP model as a first guess. The probability estimation of the neural network wind directions is explicitly introduced as a constraint in the adapted version of PRESCAT. After disambiguation, the correct direction is retrieved 89% of the time. Due to the high skill of the first alias provided by NN-INVERSE model, we can envisage a self-consistent neural network ambiguity removal method similar to this proposed in Badran *et al* (1991). These authors showed that with 25% of ambiguous wind direction, 99 % of them were corrected with the NN approach. Thanks to the good performances displayed in **Tab. 2** for the direction, we can thus envisage to remove the ambiguity without any external information.

Systematic comparisons with other methods have been processed. It appears that the NN has a very good skill. The advantages of the neural network method are linked to:

- their ability of modeling non-linear phenomena that do not assume the forms of the functions and noises involved in the physical processes,

- the ability to use a spatial context which improves greatly the performance of the first alias solution and thus the skill of any ambiguity removal algorithm.

- the ability to directly estimate the posterior probability of the different wind aliases with neural networks working in classifier mode. Those probabilities enhance the skill of the disambiguation phase.

Owing to its good performances the neural networks methodology is an efficient alternative for scatterometer wind field retrieval. The fact that NN-INVERSE only does algebraic operations is a major advantage for operational use.

Acknowledgements

We would like to thank the CERSAT/IFREMER who provided the collocations between ERS1 sigma-0 and the analyzed wind vectors of the ECMWF Model. We also thank D. Cornford for stimulating and enlightening discussions. The present study was supported by the EC program NEUROSAT (ENV4-CT96-0314).

References

Badran, F., S. Thiria, and M. Crepon: Wind ambiguity removal by the use of neural network techniques. *J. Geophys. Res.,* 96, 20521-20529, 1991.

Bishop, C. M.: Neural Networks for pattern recognition, *Oxford University Press*, 482 p., 1995.

Cavanié, A., and D. Offiler : ERS1 Wind Scatterometer: Wind Extraction and Ambiguity Removal. *Proc. of IGARSS 86 Symposium, Zurich,* (ESA SP-254), 1986.

Mejia, C., S. Thiria, F. Badran, and M. Crépon, A Neural Network Approach for Wind Retrieval from the ERS-1 Scatterometer Data, *IEEE Ocean94 Proc.*, Brest-Sept. 13-16 (1), 1994.

Offiler D. : The Calibration of ERS1 Satellite scatterometer winds. *J. Atm. Ocean Tech..,* 1002-1017, 1994

Quilfen, Y. and A. Bentamy : Calibration/Validation of ERS-1 scatterometer precision, *Proc. of IGARSS 94*, Pasadena, United States, 945-947, 1994.

Richard, M. D. and R. P. Lippman : Neural Network Classifiers Estimate Bayesian a posteriori Probabilities, *Neural Computation,* 3, 461-483, 1991

Rufenach, C. : Comparison of Four ERS-1 Scatterometer Wind retrieval Algorithms with buoys measurements. *J. Atm. Ocean Tech..,* 304-313, 1998.

Stoffelen, A and D. Anderson :The ECMWF Contribution to the Characterization, Interpretation, Calibration and Validation of ERS-1 Scatterometer Backscatter Measurements, and Winds, and their use in Numerical Weather Prediction Models , ESA Contract Reports, 1995.

Stoffelen, A and D. Anderson : Scatterometer data interpretation: Measurement Space and Inversion. *J. Atm. Ocean Tech..,* 1298-1313, 1997a.

Stoffelen, A and D. Anderson : Scatterometer data interpretation: Estimation and validation of the transfer function CMOD4. *J. Geophys. Res.* 102, 5767-5780, 1997b.

Stoffelen, A and D. Anderson : Ambiguity removal and assimilation of scatterometer. *Q. J. Roy. Meteorol. Soc. 123, 491-518*, 1997c

Thiria, S., F. Badran, C. Mejia and M. Crepon : A Neural Network Approach for modelling Non Linear Transfer functions : Application for Wind Retrieval from Spaceborne Scatterometer Data. *J. Geophys. Res.* 98, 22827-22841, 1993.

APPENDIX 1

The bias, standard deviation an RMS are defined as:

$$\overline{BIAIS} = \frac{\sum_i \left(val_i^c - val_i^M \right)}{N} \qquad \overline{BIAIS} = \frac{\sum_i \left(val_i^c - val_i^M \right)}{N} \qquad RMS = \sqrt{\frac{\sum \left(val_i^c - val_i^M \right)^2}{N}}$$

where val^{est} represents an estimate, val^{ref} the true value, and N is number of data..

Lest us define res_j as $res_j = val_j^{est} - val_j^{ref}$.

For wind vectors the residual and the bias are also vectors and their algebraic values are given by a norm in R^2.

For wind direction $\begin{cases} \text{if } val_j^{est} - val_j^{ref} < -180 \text{ then } res_i = val_j^{est} - val_j^{ref} + 360 \\ \text{if } val_j^{est} - val_j^{ref} > 180 \text{ then } res_i = val_j^{est} - val_j^{ref} - 360 \\ \text{else } res_i = val_j^{est} - val_j^{ref} \end{cases}$

The Perf@20° performances is the percentage of agreement between the estimated wind direction and the reference wind direction : $Perf@20° = 100 \frac{Cardinal\left\{ \left| res_j \right| < 20° \right\}}{N}$, with the same definition as for the residuals of wind direction.

APPENDIX 2

Figure of Merit (FoM)

This non-dimensional number has been proposed by D Offiler (1994) for evaluating the performances of the scatterometer retrieved winds. It is of the form:

$$\mathrm{FoM} = \frac{F_1 + F_2 + F_3}{3}$$

with

$$F_1 = \frac{40}{|v_{bias}| + 10v_{stdv} + |\chi_{bias}| + \chi_{stdv}};\ F_2 = \frac{1}{2}\left(\frac{2}{v_{rms}} + \frac{20}{\chi_{rms}}\right);\ F_3 = \frac{4}{\mathbf{V}_{rms}}$$

Where v is the wind speed, θ is the wind azimuth and $\vec{V}$ the wind vector.

These numbers are computed with the residuals defined in **Appendix 1** except for wind vector RMS V_{rms} which is defined with the following residual: $\mathbf{V}_{res} = \sqrt{\mathbf{V}_d^2 + \mathbf{V}_{ecmwf}^2 - 2\mathbf{V}_d^2\mathbf{V}_{ecmwf}^2 \cos(\chi_{res})}$.

Assuming bias free estimators, FoM = 1 if specifications of ±2m/s in wind speed error and ±20° in wind direction error are exactly fulfilled. The greater FoM, the better the inverse wind field.